Accepted Manuscript

Zhixiong Capsule (ZXC), a Traditional Chinese patent medicine, prevents atherosclerotic plaque formation in rabbit carotid artery and the related mechanism investigation based on network pharmacology and biological research

Jianxiu Zhai , Zehai Song , Yuwei Wang , Mingshu Han , Zhaohui Ren , Na Han , Zhihui Liu , Jun Yin
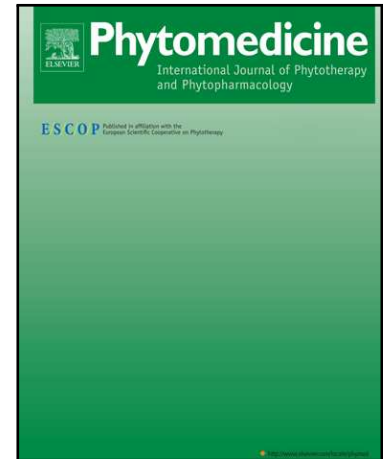
Please cite this article as: Jianxiu Zhai , Zehai Song , Yuwei Wang , Mingshu Han , Zhaohui Ren , Na Han , Zhihui Liu , Jun Yin , Zhixiong Capsule (ZXC), a Traditional Chinese patent medicine, prevents atherosclerotic plaque formation in rabbit carotid artery and the related mechanism investigation based on network pharmacology and biological research, *Phytomedicine* (2018), doi: https://doi.org/10.1016/j.phymed.2018.11.036

Zhixiong Capsule (ZXC), a Traditional Chinese patent medicine, prevents atherosclerotic plaque formation in rabbit carotid artery and the related mechanism investigation based on network pharmacology and biological research

Jianxiu Zhai, Zehai Song, Yuwei Wang, Mingshu Han, Zhaohui Ren, Na Han, Zhihui Liu, Jun Yin[a]

School of Traditional Chinese Material, Shenyang Pharmaceutical University, Shenyang 110016, China

Corresponding author.
Prof. Jun Yin
Shenyang Pharmaceutical University
103 Wenhua Road, Shenhe district
Tel: +86 24 23986491; fax: +86 24 23986460

Abstract

Background and aims: Chinese patent medicine Zhixiong Capsule (ZXC) has been used in clinical treatment against blood stasis-induced dizziness and headache for many years in China.

Hypothesis/Purpose: Recent clinical observations demonstrated a good efficacy of ZXC against atherosclerotic plaque formation in carotid arteries. The aims of this study were to verify the plaque-preventing efficacy of ZXC in animals and to investigate the underlying mechanisms.

Study design/Methods: ZXC (185 mg/kg and 370 mg/kg) was administrated to rabbits which received collar implantation accompanied with high fat diet administration (12 d). The blood-dissolved components of ZXC were identified by an UPLC-QTOF-MS method. The key components and targets of ZXC were then predicted based on network pharmacology analysis and biological investigations.

Results: Compared with vehicle control group, ZXC administration (185 mg/kg) significantly prevented plaque formation and attenuated intima thickening in the collar-implanted carotid arteries, markedly decreased blood lipid level, and increased plasma IL-4 level in rabbits. A total of 23 blood-dissolved components were identified. Four ingredients (namely, kaempferol, daidzein, puerarin, miltirone) along withleech, and three targets (namely, JUN, FOS and TP53) were recognized to play important roles for ZXC bioactivity.

Conclusions: It could be concluded that ZXC could be applied to prevent atherosclerotic plaque formation and intimal thickening in carotid arteries at the current clinical dose.

Key words: Zhixiong Capsule, atherosclerotic plaque, network pharmacology, TP53, JUN, FOS

Abbreviations

Atherosclerosis, AS; Average shortest pathway length, ASPL; Betweeness centrality , BC; Binding Database, BD; hematoxylin-eosin, HE; High density lipoprotein cholesterol, HDL-C; Interleukin-4, IL-4; Interleukin-13, IL-13; Kyoto Encyclopedia of Genes and Genomes, KEGG; Low density lipoprotein cholesterol, LDL-C; Oxidative LDL, Ox-LDL; Malondialdehyde, MDA; Online Mendelian Inheritance in Man, OMIM; Superoxide dismutase, SOD; Total cholesterol, TC; Traditional Chinese Medicine Systems Pharmacology, TCMSP; Triglyceride, TG; Tumor necrosis factor alpha, TNF-α; Therapeutic Target Database, TTD; Zhixiong capsule, ZXC.

Introduction

Plaque formation plays a vital role in the pathogenesis of atherosclerosis (AS) (Davis, 2005). As atherosclerotic plaque develops, there is a risk for plaque rupture, which would lead to thrombus formation and even vascular occlusion (Chen et al., 2016) . In carotid arteries, plaque rupture could result in severe fatal events such as stroke and cerebral infarction (De Boer et al., 2015; Li et al., 2014). To avoid such events, AS patients usually have to receive medical or surgical treatments while suffering from the accompanied side effects: the anti-coagulation agents could lead to gastric mucosa injury (Bastaki et al., 2017; Kato et al., 2016), the lipid-lowering agents may result in hepatotoxicity and nephrotoxicity (Bastaki et al., 2017; Shahrbaf and Assadi, 2015), and there is a risk of secondary thrombosis for those who received surgical intervention (Mücke et al., 2016). Recently, Chinese medicines have been found with good efficacy in the treatments against cardiovascular diseases with their multi-component, multi-target, multi-pathway strategies, and thus may cause less side effects if applied properly (Yu et al., 2013; Zheng et al., 2016).

Chinese patent medicine Zhixiong Capsule (ZXC) has been used in clinical treatment against blood stasis-induced dizziness and headache for many years (Hua and Xing, 2003; Xing and Yonghong, 1998). ZXC is composed of leech, *Ligusticum chuanxiong*, *Salvia miltiorrhiza*, *Leonurus artemisia*, and *Pueraria lobata*. Among the five materials, *L. chuanxiong* and leech are generally considered as the primary materials against blood stasis with their representative components, namely ligustrazine and hirudin (Mu?Oz et al., 2015; Wang et al., 2016). Meanwhile, *Salvia miltiorrhiza*, *Leonurus artemisia*, and *Pueraria lobata* have been found with significant antioxidant, anti-inflammatory and cardiovascular-protective properties (Jiang et al., 2015; Wu et al., 2007; Zhou et al., 2015). While recently applied in clinical treatments, it was found that ZXC showed good efficacy in preventing atherosclerotic plaque formation in carotid arteries. The observation demonstrated an extensive clinical value of ZXC, which has not been investigated elsewhere.

To verify the plaque-preventing effects of ZXC in carotid arteries and to

5

investigate the underlying mechanisms, a series of experiments were carried out in this study: the plaque-preventing effect of ZXC was validated in a rabbit model, the key ingredients and targets of ZXC were identified by network pharmacology analysis and biological investigations. At last, the potential mechanisms of ZXC bioactivities were raised for further studies.

Materials and methods

Chemicals and reagents

Zhixiong capsule (ZXC, batch No. 171103) was obtained from Qianhui Co., Ltd. (Taiyuan, China). High fat diet was obtained from Jiemin Col, Ltd. (Nanjing, China). Total cholesterol (TC), triglyceride(TG), high density lipoprotein cholesterol (HDL-C), low density lipoprotein cholesterol (LDL-C), malondialdehyde (MDA), superoxide dismutase (SOD) assay kits were obtained from Nanjing Jiancheng Bioengineering Institute (Nanjing, China). Tumor necrosis factor alpha (TNF-α), interleukin-4 (IL-4) and interleukin-13 (IL-13) Elisa Kits were purchased from Meimian Biotechnology Institute (Shenyang, China).

HPLC qualitative analysis of ZXC

Puerarin was considered as a main active component in ZXC, and its content was determined according to the method of our previous study with slight modifications (Zhou et al., 2018) . Briefly, ZXC was dissolved in MeOH at a concentration of 1 mg/mL and filtered (0.22 μm) before HPLC analysis. An Agilent ZORBAX SB-C18 column (4.6 mm×250 mm, 5 μm) was employed for component separation, the column temperature was set at 25 °C. The binary gradient elution system was composed of (A) acetonitrile and (B) 0.1% formic acid, the elution gradient was set as follows: 0–10 min,10–15% A;10–20 min, 15–25% A; 20–30 min, 25–35% A; 30–40 min, 35–45% A; 40–50 min, and 45–60% A. The flow rate was set at 0.8 ml/min. The injection volume was 10 μl and the wavelength was 254 nm.

Animal preparation

Male Japanese rabbits weighing 2 kg–2.5 kg were used in the study. Rabbits

were obtained from the animal experimental center of Shenyang Pharmaceutical University (Liaoning, RP China). All experimental protocols were in accordance with the guidelines approved by the animal ethical committee of Shenyang Pharmaceutical University (approval number: SYPU-IACUC-C2017-1022-177).

Experimental design

Forty rabbits were randomly assigned into four groups (G1–4, n=10). For acclimation, all rabbits were housed individually in steel mesh cages under standard conditions at the animal experimental center with standard rabbit chow and water ad libitum (Liaoning changsheng biotechnology co. LTD, Shenyang, China) for 7 d.

As shown in supplement Fig. 1, G 1 was set as blank control group and were fed with standard diet all along. After acclimation, rabbits in G 2–G 4 received silica collar implantation surgery. Briefly, rabbits in G 2–G 4 were anesthetized by 10% chloral hydrate (2 ml/kg). After anesthesia, an incision along the midline of neck was made, both carotid arteries were exposed and separated from surrounding tissues. A non-occlusive silastic collar (total length 20 mm; internal diameter 1.5 mm; external diameter 3 mm) was then positioned around the right carotid artery, according to standard procedures (Booth et al., 1989) . For each animal, the left carotid artery (non-operated) was sham operated by positioning the silica collar around the artery and removing the collar before artery reseating and suture. All rabbits were kept for another 7 d for wound healing after the surgery. At the 8th day, rabbits in G 2–G 4 began receiving high-fat diet (2% cholesterol, 4% lard) for 12 d. During the same period, rabbits in G 2–G 4 received saline or ZXC intragastric administration. G 2: vehicle control group, rabbits received intragastric saline administration (5 ml/kg, once a day). G 3: ZXC-low dose group (ZXC-L), rabbits were administrated with ZXC at the dose of 185 mg/kg for 12 consecutive days (once a day, i.g.). G 4: ZXC-high dose group (ZXC-H), rabbits were administrated with ZXC at the dose of 370 mg/kg for 12 d (once a day, i.g.). The dosages of ZXC were designed based on clinical application.

At the 0 d, 3 d, 6 d, 9 d and 12 d of high-fat diet administration, blood samples

7

were collected from rabbits after fasting for 12 h. The blood samples were then centrifuged at 4000 rpm for 10 min to obtain plasma, which were stored at $-80℃$ until use. At the 12 d, rabbits were sacrificed with overdose chloral hydrate, and the carotid arteries were collected, quickly washed in cool saline, and were divided from the surrounding tissue. In each group (n=10), rabbits were then randomly separated into two subgroups (n=5). The carotid arteries of the first subgroup were used for Sudan IV staining. For the second subgroup, the upper halves of the carotid arteries were used for histological investigation (HE or masson-trichrome staining) . The lower halves of the carotid arteries were used for oxidative stress level assessment (MDA and SOD) (supplement Fig. 1).

Histological analysis

After collected and washed, a proportion of the carotid arteries (supplement Fig. 1) were immediately fixed in 10% formalin-saline solution and kept for 24 h. Samples from the first subgroups were then used for Sudan IV staining. Samples from the second subgroups were embedded in paraffin and cut into slices (5 μm thickness), sections were treated with hematoxylin-eosin (HE) and masson's trichrome staining.

The specimens were further observed and photographed under a light microscope equipped with a digital camera (Olympus BX51TF, Tokyo, Japan). The area of atherosclerotic plaque (Sudan IV staining) as well as the cross-section area of intima and media (HE staining) were measured by cellSens Standard 1.4.1 software (Olympus, Japan). Then the ratio of atherosclerotic area to the whole carotid artery area (Sudan IV staining) and the ratio of intimal cross-section area to medial cross-section area were calculated.

Analysis of plasma lipids

Plasma TC, LDL-C, HDL-C and TG levels were measured using assay kits (Nanjing, China).

Analysis of oxidative stress level in carotid arteries

The oxidative stress level in carotid arteries was assessed by measuring MDA content and SOD activity. Briefly, carotid arteries were cut into small fragments and

8

mixed with 10-fold volume of cool saline. The mixture was then homogenized at 4 ℃, the homogenate was centrifuged at 4000 rpm for 10 min (4 ℃), and the supernatant was then assessed with assay kits (Nanjing, China).

Effects of ZXC on rabbit plasma TNF-α, IL-4 and IL-13 levels

The determination of IL-4 and IL-13 levels were designed according to pathway analysis results (see below in result, pathway analysis and in Table 1. (C)). The levels of TNF-α, IL-4 and IL-13 levels in rabbit plasma were determined using commercially available ELISA kits. The plasma samples were collected and prepared at the 12 d of high-fat diet administration. The concentration of TNF-α, IL-4 and IL-13 are expressed as pg/ml.

Serum collection and preparation

To determine the components which actually entered blood circulation after ZXC administration, serum were collected, prepared and determined by LC-MS method. Briefly, three rabbits were administrated (i.g.) with ZXC (370 mg/kg). Thirty minutes after administration, blood was collected from the ear vein and then placed for coagulation at 37 ℃ for 30 min. Serum from three rabbits was then equally mixed (1:1:1) after centrifuged (5000 rpm, 15 min) separately. After that, 1.4 ml serum was mixed with 14 ml of extract liquor (diethyl ether: ethyl acetate: methanol=1:4:1) and then vortexed for 1 min. The mixture was then centrifuged (5000 rpm, 15 min), evaporated to dryness, and finally dissolved into 400 μl methanol. The methanol solution was centrifuged twice at 12000 rpm (10 min each time), and the supernatant was used for MS determination.

Blood-dissolved ZXC component identification

A Waters ACQUITY UPLC system (Waters Corporation, Milford, MA, USA) coupled to a Waters Xevo G2QTOF mass spectrometer (Waters MS Technologies, Manchester, UK) was used for analyzation. The UPLC consisted of a quaternary solvent pump and a sample manager. A Welch Ultimate UPLC XB-C18 Column (2.1×100 mm, 1.8 μm) was used for elution with a constant flow rate of 0.3 ml/min at 30 °C. For each run, 10 μl sample was injected and eluted with solvent A (0.1%

formic acid) and solvent B (acetonitrile) as the following gradient: 0-10 min, 10-70% B; 10-15 min, 70-95% B; 15-20 min, 95% B. For each sample, spectra were acquired in both the positive and negative ionization modes, with the capillary voltage set at -3000 V and +2500 V. After the UPLC-QTOF/MS determination, the raw data collected in positive and negative modes were further processed using a MassLynx 4.1 workstation (Waters, USA).

Target collection

A flow chart for internal study design could be found in supplementary file. As shown in supplement Fig. 2, AS-related genes were obtained using the Traditional Chinese Medicine Systems Pharmacology Database (TCMSP, http://lsp.nwu.edu.cn/tcmsp.php), Online Mendelian Inheritance in Man Database (Hamosh et al., 2005) (OMIM, http://www.omim.org/), Therapeutic Target Database (Yang et al., 2016) (TTD, https://db.idrblab.org/ttd/), Drugbank Database (Wishart et al., 2017) (https://www.drugbank.ca/), Kyoto Encyclopedia of Genes and Genomes Database (Kanehisa and Goto, 2000) (KEGG, https://www.kegg.jp/). The targets of the blood-dissolved ZXC components were collected from the TCMSP Database (Ru et al., 2014) Binding Database (Liu et al., 2007) (BD, http://www.bindingdb.org/bind/index.jsp), TTD, KEGG Database. In addition, leech was considered as an integrity during target collection, and its related targets were collected according to previous literatures (Dong et al., 2016; Wu and Yang, 2018; Wu et al., 2017). The overlapped targets that were both related to atherosclerosis and the components were collected for further network construction and analysis (supplement Fig. 2).

Protein-protein interactions (PPIs)

STRING database (http://string-db.org/) was employed to identify the possible inter-protein interactions (PPIs) (Szklarczyk et al., 2017). To improve the reliability of the achieved data, the PPIs were further filtered with the minimum combine score of 0.98 (very high confidence), and the remained PPIs were used for network construction and analysis.

Network construction and analysis

The chemical-target network and PPIs network were constructed using Cytoscape software (version 3.2.1) (Shannon et al., 2003). After network construction, the parameters such as average shortest pathway length (ASPL) and betweeness centrality (BC) were calculated by Network Analyzer (De et al., 2003). In addition, the PPIs network was further analyzed using cytohubba, a Cytoscape plug-in, to identify the hub targets (Chin et al., 2014).

Pathway analysis

Reactome, a plug-in of Cytoscape, was used for pathway enrichment analysis (LIGTENBERG and HILBERS, 2013).

Result

HPLC quantitative analysis of ZXC

In our previous study, and the main components in ZXC (batch No. 160401) was identified by MS detection, and the main effective component puerarin was quantified as 33.23 mg/g by HPLC method (Zhou et al., 2018). The ZXC (batch No. 171103) used in this study was found with a puerarin content of 30.58 mg/g, which is similar to batch No. 160401 (supplement Fig 3).

Histological analysis

The representative results of HE staining, masson-trichrome staining and Sudan IV staining were shown in Fig. 1. With the combination of collar-implantation and high fat diet administration, the right carotid arteries of rabbits in vehicle control group were severely covered by AS plaque, and were occupied with foam cells and collagen (Fig. 1 (A)(b), (B)(b) and (E)(b)). Compared with vehicle control group, low-dose and high-dose ZXC administration significantly prevented plaque formation in collared carotid arteries by 78.2% and 72.9%, respectively (Fig. 1 (A) and (B)). The representative results of HE staining (Fig. 1 (C) and (D)) revealed a statistically significant intimal-thickening in rabbits compared with vehicle control group. By ZXC administration (185 mg/kg and 370 mg/kg), the intimal-thickening was

11

remarkably attenuated, and the ratio of intima/media area was reduced by 88.1% and 92.3%, respectively (p<0.01).

Analysis of plasma lipids

To reflect the changes in plasma lipid level throughout the experiment, plasma TC, TG, HDL-C and LDL-C contents were evaluated at 0 d, 3 d, 6 d, 9 d and 12 d of high-fat diet administration. The evaluation results were summarized in supplement Table 1 and were presented in Fig. 2. At 12 d, the blood lipid level of vehicle control group significantly increased compared with blank control group: the TC level, TC/HDL-C ratio and log(TG/HDL-C) value was increased by 2.3-, 5.8- and 2.4-fold, respectively (p<0.01), and the plasma HDL-C content was decreased by 51% (p<0.01). ZXC low-dose administration (185 mg/kg) showed a significant lipid-lowering effect compared with vehicle control group: the TC level, TC/HDL-C ratio and log(TG/HDL-C) value was decreased by 89.3%, 54.4% and 90.3%, respectively (p<0.01), and the plasma HDL-C content was increased by 2.6-fold (p<0.01). ZXC high-dose administration (370 mg/kg) showed a weaker blood lipid-lowering effect: compared with vehicle control group, the TC level ,TC/HDL-C ratio and log(TG/HDL-C) value was decreased by 64.2%, 80.3%, and 72.0%, respectively (p<0.01), and the HDL-C content was increased by 1.6-fold (p<0.05).

Analysis of oxidative stress level in carotid arteries

As shown in Fig. 3 (A) and (B), low dose ZXC administration showed a mild effect on reducing MDA level (no statistical significance), yet low dose or high dose ZXC showed little effect on increasing SOD activity. The collared carotid arteries from all groups demonstrated higher MDA content along with lower SOD activity compared with the sham-operated carotid arteries.

Effects of ZXC on rabbit plasma IL-4, IL-13 and TNF-α levels

TNF-α, IL-4 and IL-13 plasma contents were determined to assess the inflammation level in experimental rabbits. The determination of IL-4 and IL-13 levels were designed according to pathway analysis results (Table 1. (C)). Rabbits in

12

ZXC-L group were observed with a 35% increase in plasma IL-4 level (Fig. 3 (C), $p<0.05$) compared with vehicle control group. In contrary, ZXC high dose administration significantly decreased IL-13 level when compared with blank and vehicle control groups (Fig. 3 (D)) ($p<0.01$). Additionally, the plasma TNF-α level of rabbits in vehicle control group showed an increasing tendency compared with blank control group, which was eliminated to some extent by ZXC-L and ZXC-H administration (Fig.3 (E)). However, the plasma TNF-α contents were statistically indifferent among four groups.

Blood-dissolved ZXC component identification

With UPLC-QTOF/MS determination, a total of 21 peaks were identified (supplement Fig. 4, supplement Table 2), namely daidzin (p1), 1,2,5,6-tetrahydrotanshinone (p2), senkyunolide J (p3), tetramethylpyrazine (p4), 3α-hydroxytanshinone Ⅱ a (p5), (6S)-6-(hydroxymethyl)-1,6-dimethyl-8,9-dihydro-7H-naphtho[8,7-g]benzofuran-10,0-dione (p5[#]), dan-shexinkum d (p6), kaempferol (n1), puerarin (n2), protocatechuic acid (n3), protocatechuic aldehyde (n4), miltirone (n5), dimethyl lithospermate (n6), neocryptotanshinone ii (n7), salvilenone Ⅰ (n8), daidzein (n9), 3'-methoxydaidzein (n10), epidanshenspiroketallactone (n10[#]), leonurine (n11), 1-methyl-8,9-dihydro-7H-naphtho[5,6-g]benzofuran-6,10,4-trione (n12), danshenspiroketallactone (n13), senkyunolide I (n14), senkyunolide H (n14[#]), quercetin (n15). Among the identified MS peaks, the molecular weight of p5, n10 and n14 were consisted with more than one candidate compounds. The additional candidates (which are marked with[#]) were also included for further network pharmacological analysis. The secondary MS spectrums are shown as supplement Fig. 5-25.

ZXC component-target network construction and topological analysis

After collection, 1917 AS-related genes were obtained from the TCMSP Database, OMIM Database, TT Database, Drugbank Database and KEGG Database. Based on the blood-dissolved ZXC components, 492 ZXC targets were obtained from

the TCMSP Database, Binding Database, TT Database, Drugbank Databse and KEGG Database. A total of 266 overlapped genes, which were both related to AS and ZXC were kept for further network construction using Cytoscape software (Fig. 4 (A)). The overlapped genes were mapped to blood-dissoved ZXC components to obtain shared components. With the analysis using Network Analyzer, the topological parameters such as shortest pathway length (ASPL) and betweeness centrality (BC) were calculated (Supplement Table 3), and the top five components with large BC and small ASPL were recognized as the key components of ZXC. As a result, four components (namely, kaempferol, daidzein, puerarin and miltirone) along with leech were considered to be the key compositions of ZXC (Table. 1 (A)). Among the ingredients, kaempferol (from herb *Leonurus artemisia*) was found with the smallest ASPL (1.74895) and largest BC (0.70023).

ZXC PPIs network construction and topological analysis

The overlapped 266 targets, which are both related to AS and plasma-contained ZXC components, were further analyzed for PPIs using STRING Database. Among the attained 3348 PPIs, 162 PPIs were found with combine scores over 0.98 (very high confidence). A total of 74 targets, which were involved in the high confident PPIs, were employed for further network construction using Cytoscape software (Fig 4 (B), supplement Table 4). With the analysis using Network Analyzer and cytohubba, JUN and TP53 were both recognized as key (hub) targets, with the betweeness centrality of 0.24642 (cytohubba rank 1) and 0.24410 (cytohubba rank 3), respectively (Table 1 (B)).

Pathway analysis

The 74 targets were further employed for pathway enrichment analysis by using Reactome plug-in to identify the potential pathways intervened by ZXC administration. A total of 63 potential pathways were obtained with a cut-off p-value of 0.001, the top five enriched pathways with smallest p-values were considered to be the most important pathways (Table 1 (C)), namely interleukin-4 (IL-4) and IL-13 signaling, activation of the AP-1 family of transcription factors, MAPK targets

mediated by MAP kinases, transcriptional regulation by TP53, and regulation of TP53 activity.

Discussion

In this study, ZXC was found to significantly prevented AS plaque formation and intimal thickening in carotid arteries of the rabbits which received collar-implantation accompanied with high-fat diet administration. On the basis of blood-dissolved ZXC ingredients, the key ingredients, potential targets of ZXC were analyzed using network pharmacological analysis. In combination with pathway enrichment analysis results, several hypothesis for possible mechanisms were raised for further studies. The dosage of ZXC was designed based on its clinical application, and the low dose in this study (185 mg/kg) is equivalent to the recommended dosage for human (3.6 g/d).

It was found that ZXC significantly prevented plaque formation in rabbit carotid arteries. As a result of collar-implantation and 12 d of high-fat diet intake, the right carotid arteries of model rabbits were severely occupied with plaque, and the intima thickened significantly with foam cells and collagens (Fig. 1). With low-dose and high-dose ZXC administration, the intima-thickening and plaque accumulation was significantly alleviated, and the results in ZXC-L and ZXC-H groups were statistically indifferent. However, low-dose ZXC administration was observed with better lipid-lowering efficacy (Fig. 2) by significantly increasing plasma HDL level and decreasing TC level. The value of log(TG/HDL-C) is a characteristic indicator for LDL particle size and for AS progression extent (Dobiášová and Frohlich, 2001). It was found that low dose ZXC administration showed better efficacy in LDL particle size compared with high dose administration. Also, it could be speculated that the lipid-lowering action of ZXC contributed significantly to its bioactivity, because the accumulation and monocyte-engulfment of LDL particles are the early events of plaque formation (Davis, 2005). By reducing blood lipid level and shrinking LDL-particle size, ZXC could inhibit plaque generation in the early stage.

15

Low-dose ZXC administration also showed better antioxidative and anti-inflammatory effects when compared with high-dose ZXC. As shown in Fig. 3 (A), the MDA levels in the operated carotid artery were significantly higher than the sham operation side, which could be caused by the continuous contact with implanted silica collar. When received low-dose ZXC, the MDA level showed a decrease trend compared with vehicle control group and high-dose ZXC group (statistically indifferent). With lower oxidative level, it could be hypothesized that rabbits from low-dose ZXC would produce less oxidative LDL (Ox-LDL) compared with those from high-dose ZXC group, leading to a lower inflammation level. The hypothesize was supported well by Fig. 3 (C-D), where the levels of anti-inflammatory cytokine IL-4 and IL-13 were found to be higher in ZXC-L group compared with ZXC-H group (Gao et al., 2015). Along with the other test results, it could be concluded that low dose ZXC administration is more appropriate for preventing AS progression compared with high dose ZXC administration.

By network pharmacology analysis, four components (kaempferol, daidzein, puerarin and miltirone) along with leech were recognized as key components of ZXC against AS progression. The significant blood lowering effect of ZXC may be contributed partly by puerarin, which was reported to significantly decreased blood cholesterol level (Yan et al., 2006). As one of the most important components in ZXC (Table 1 (A)), puerarin was also found with other beneficial properties, such as suppressing inflammation, inhibiting vascular smooth muscle cell (VSMC) proliferation and alleviating pain (Kim et al., 2010; Ullah et al., 2018; Wan et al., 2018). The cardiovascular-protective properties of the other key components (and leech) could also be evidenced by previous investigations, such as anticoagulation (kaempferol and leech)(Tsoucalas et al., 2016; Wang et al., 2015), anti-inflammation (kaempferol, daidzein, and mitirone) (Devi et al., 2015; Makishima et al., 2016; Wang et al., 2017), and inhibiting VSMC migration (miltirone and leech) (Li et al., 2017; Song et al., 2018). Interestingly, puerarin, miltirone and kaempferol were recently reported with protective effects against ox-LDL induced oxidative stress and cell

damage, which could be of great value in blocking plaque development (Che et al., 2017; Deng et al., 2017; Zhang et al., 2016).

Based on the results attained from network pharmacology analysis as well as biochemistry analysis, the possible mechanisms for the curative effect of ZXC against plaque formation were discussed as follows. The first possible mechanism is that ZXC might alleviate inflammation by regulating JUN and FOS expressions. By using Network Analyzer, JUN was recognized as the most important target of ZXC with the smallest ASPL and the largest BC (Fig. 4 (B)(a)). The significance of JUN was also agreed by cytohubba analysis result (Fig. 4 (B)(b), Table 1 (B)), which was attained with a more balanced and complexed methodological strategy (Chin et al., 2014). Interestingly, cytohubba analysis identified FOS as the second-important hub target (rank 2), which is bio-functionally associated with JNK in the inflammation process (Yang et al., 2017). The encoded proteins of JUN and FOS, c-fos and c-jun, would combine and form activator protein-1 (AP-1)(Hess et al., 2004). AP-1 would then trigger inflammation by inducing proinflammatory genes and thus increase the expression of inflammatory cytokines, such as TNF-α, cyclo-oxygenase-2 (COX-2), and interleukin-1 beta (IL-1β) (Adamopoulos et al., 2015). The above results indicated that ZXC may alleviate the inflammation in rabbit models by down-regulating JUN and FOS expression, decreasing AP-1 production and thus block the downstream inflammatory reactions. This hypothesis was also supported by the reactome pathway analysis results, in which "AP-1 family activation" was considered of great importance for ZXC efficacy (Table 1 (C)).

The second possible mechanism is that ZXC may inhibit the differentiation from embryonic stem cells (ESCs) to vascular smooth muscle cells (VSMCs) by down-regulating TP53 expression. TP53 was identified as one of the key targets by Network Analyzer and cytohubba analysis in this study (Fig. 4 (B)(b), Table 1 (B)), and has been recently recognized to closely participate in the process of AS plaque formation and development. A significant TP53 overexpress has been observed recently in the plaque area(Blin et al., 2013; Zawada et al., 2012), which could be

17

associated with the abnormal vascular smooth muscle cell (VSMC) differentiation. With the stimulation of increased inflammatory factors in the plaque forming area, part of the embryonic stem cells (ESC) would differentiate into VSMC to further participate in plaque formation and progression (Du et al., 2012). It was reported by Tan et al. that p53, the protein encoded by TP53, could significantly promote the differentiation from ESCs to VSMCs (Tan et al., 2018). With the above observations, it could be speculated that ZXC may down regulate TP53 expression in plaque area, inhibit the differentiation from ESCs to VSMCs, and thus prevent plaque formation.

However, there are limitations in this study. In further studies, the above key targets of ZXC are to be verified by *in vivo* and *in vitro* experiments, and the connection between targets and ZXC components will be further investigated.

Conclusion

In this study, it was found that low-dose ZXC (185 mg/kg) significantly attenuated AS in rabbits, markedly down-regulated blood lipid level and increased anti-inflammatory cytokine IL-4 level. Network pharmacological analysis results indicated that JUN, FOS and TP53 may be the key targets of ZXC, and ZXC may intervene AS progression by inhibiting VSMC dedifferentiation and blocking pro-inflammation process. It could be concluded that low-dose ZXC could be applied as an anti-AS agent in clinic.

Conflict of interest

This research does not have any conflict of interest with anyone or any institute.

References

Adamopoulos, C., Piperi, C., Gargalionis, A.N., Dalagiorgou, G., Spilioti, E., Korkolopoulou, P., Diamanti-Kandarakis, E., Papavassiliou, A.G., 2015. Advanced glycation end products upregulate lysyl oxidase and endothelin-1 in human aortic endothelial cells via parallel activation of ERK1/2–NF-κB and JNK–AP-1 signaling

pathways. Cell. Mol. Life Sci. 73, 1685-1698.

Bastaki, S.M.A., Padol, I.T., Amir, N., Hunt, R.H., 2017. Effect of Aspirin and ibuprofen either alone or in combination on gastric mucosa and bleeding time and on serum prostaglandin E 2 and thromboxane A 2 levels in the anaesthetized rats in vivo. Mol. Cell. Biochem. 97, 1-10.

Blin, J., Ahmad, Z., Rampal, L.R., Mohtarrudin, N., Tajudin, A.K., Adnan, R.S., 2013. Preliminary assessment of differential expression of candidate genes associated with atherosclerosis. Genes Genet. Syst. 88, 199-209.

Booth, R.F., Martin, J.F., Honey, A.C., Hassall, D.G., Beesley, J.E., Moncada, S., 1989. Rapid development of atherosclerotic lesions in the rabbit carotid artery induced by perivascular manipulation. Atherosclerosis 76, 257-268.

Che, J., Liang, B., Zhang, Y., Wang, Y., Tang, J., Shi, G., 2017. Kaempferol alleviates ox-LDL-induced apoptosis by up-regulation of autophagy via inhibiting PI3K/Akt/mTOR pathway in human endothelial cells. Cardiovasc. Pathol. 31, 57-62.

Chen, Y.C., Huang, A.L., Kyaw, T.S., Bobik, A., Peter, K., 2016. Atherosclerotic Plaque Rupture: Identifying the Straw That Breaks the Camel's Back. Arteriosclerosis Thrombosis & Vascular Biology 36, e63.

Chin, C.H., Chen, S.H., Wu, H.H., Ho, C.W., Ko, M.T., Lin, C.Y., 2014. cytoHubba: identifying hub objects and sub-networks from complex interactome. BMC Syst. Biol. 8, S11.

Davis, N.E., 2005. Atherosclerosis--an inflammatory process. J. Insur. Med. 37, 72.

De Boer, O.J., Van, d.W., Allard C, Becker, A.E., 2015. Atherosclerosis, inflammation, and infection. J. Pathol. 190, 237-243.

De, J.H., Geiselmann, J., Hernandez, C., Page, M., 2003. Genetic Network Analyzer: qualitative simulation of genetic regulatory networks. Bioinformatics 19, 336-344.

Deng, H.F., Wang, X.L., Sun, H., Xiao, X.Z., 2017. Puerarin inhibits expression of tissue factor induced by oxidative low-density lipoprotein through activating the PI3K/Akt/eNOS pathway and inhibiting activation of ERK1/2 and NF-kappaB. Life Sci. 191, 115-121.

19

Devi, K.P., Malar, D.S., Nabavi, S.F., Sureda, A., Xiao, J., Nabavi, S.M., Daglia, M., 2015. Kaempferol and inflammation: From chemistry to medicine. Pharmacol. Res. 99, 1-10.

Dobiášová, M., Frohlich, J., 2001. The plasma parameter log (TG/HDL-C) as an atherogenic index: correlation with lipoprotein particle size and esterification rate inapoB-lipoprotein-depleted plasma (FER HDL). Clin. Biochem. 34, 583-588.

Dong, H., Ren, J.X., Wang, J.J., Ding, L.S., Zhao, J.J., Liu, S.Y., Gao, H.M., 2016. Chinese Medicinal Leech: Ethnopharmacology, Phytochemistry, and Pharmacological Activities. Evid. Based Complement. Alternat. Med. 2016, 7895935.

Du, J., Teng, R.J., Guan, T., Eis, A., Kaul, S., Konduri, G.G., Shi, Y., 2012. Role of autophagy in angiogenesis in aortic endothelial cells. American Journal of Physiology Cell Physiology 302, C383.

Gao, S., Zhou, J., Liu, N., Wang, L., Gao, Q., Wu, Y., Zhao, Q., Liu, P., Wang, S., Liu, Y., Guo, N., Shen, Y., Wu, Y., Yuan, Z., 2015. Curcumin induces M2 macrophage polarization by secretion IL-4 and/or IL-13. J. Mol. Cell. Cardiol. 85, 131-139.

Hamosh, A., Scott, A.F., Amberger, J., Bocchini, C., Valle, D., Mckusick, V.A., 2005. Online Mendelian Inheritance in Man (OMIM), a knowledgebase of human genes and genetic disorders. Nucleic Acids Res. 33, 514-517.

Hess, J., Angel, P., Schorppkistner, M., 2004. AP-1 subunits: quarrel and harmony among siblings. J. Cell Sci. 117, 5965-5973.

Hua, T., Xing, W., 2003. Study on 60 cases of cerebral infarction treated with Zhixiong Capsule. Journal of Nantong University 23, 304-304 (in Chinese).

Jiang, Y., Wang, L., Li, Z., Wang, T., Zhou, Y., Ding, C., Yang, R., Wang, X., Lin, Y., 2015. Optimization of extraction and antioxidant activity of polysaccharides from Salvia miltiorrhiza Bunge residue. Int. J. Biol. Macromol. 79, 533-541.

Kanehisa, M., Goto, S., 2000. KEGG: Kyoto Encyclopedia of Genes and Genomes. Nucleic Acids Res. 27, 29-34.

Kato, H., Nakazawa, Y., Kurokawa, Y., Kashiwagi, H., Morikawa, Y., Morita, D., Banno, F., Honda, S., Kanakura, Y., Tomiyama, Y., 2016. Human CalDAG-GEFI

deficiency confers severe bleeding tendency and delayed αIIbβ3 activation velocity. Blood.

Kim, K.M., Jung, D.H., Jang, D.S., Kim, Y.S., Kim, J.M., Kim, H.N., Surh, Y.J., Kim, J.S., 2010. Puerarin suppresses AGEs-induced inflammation in mouse mesangial cells: a possible pathway through the induction of heme oxygenase-1 expression. Toxicol. Appl. Pharmacol. 244, 106-113.

Li, H., Horke, S., Forstermann, U., 2014. Vascular oxidative stress, nitric oxide and atherosclerosis. Atherosclerosis 237, 208-219.

Li, S., Cheng, L., An, D., Song, S., Liang, H., Chu, F., Ji, A., 2017. Whitmania Pigra Whitman Extracts Inhibit Lipopolysaccharide Induced Rat Vascular Smooth Muscle Cells Migration and their Adhesion Ability to THP-1 and RAW 264.7 Cells. Journal of Atherosclerosis and Thrombosis 24, 301-311.

LIGTENBERG, W.P.A., HILBERS, P.A.J., 2013. RECONN: A CYTOSCAPE PLUG-IN FOR EXPLORING AND VISUALIZING REACTOME. J. Bioinform. Comput. Biol. 11, 1350004-.

Liu, T., Lin, Y., Wen, X., Jorissen, R.N., Gilson, M.K., 2007. BindingDB: a web-accessible database of experimentally determined protein–ligand binding affinities. Nucleic Acids Res. 35, 198-201.

Mücke, T., Wolff, C., Von, D.M., Mitchell, D.A., Ritschl, L.M., Fichter, A.M., 2016. Form and Size Matter: Increased Risk of Thrombosis in Microvessels with Surgically Created Endothelial Lesions. J. Reconstr. Microsurg. 33, 040-044.

Makishima, M., Sakamoto, Y., Kanatsu, J., Toh, M., Naka, A., Kondo, K., Iida, K., 2016. The Dietary Isoflavone Daidzein Reduces Expression of Pro-Inflammatory Genes through PPARα/γ and JNK Pathways in Adipocyte and Macrophage Co-Cultures. PLoS One 11, e0149676.

Mu?Oz, M.C., Montes, R., ., Hermida, J., ., Orbe, J., ., Páramo, J.A., Rocha, E., . 2015. Effect of the administration of recombinant hirudin and/or tissue-plasminogen activator (t-PA) on endotoxin-induced disseminated intravascular coagulation model in rabbits. Br. J. Haematol. 105, 117-121.

Ru, J., Li, P., Wang, J., Zhou, W., Li, B., Huang, C., Li, P., Guo, Z., Tao, W., Yang, Y., Xu, X., Li, Y., Wang, Y., Yang, L., 2014. TCMSP: a database of systems pharmacology for drug discovery from herbal medicines. J. Cheminform. 6, 13.

Shahrbaf, F.G., Assadi, F., 2015. Drug-induced renal disorders. Journal of Renal Injury Prevention 4, 57-60.

Shannon, P., Markiel, A., Ozier, O., Baliga, N.S., Wang, J.T., Ramage, D., Amin, N., Schwikowski, B., Ideker, T., 2003. Cytoscape: a software environment for integrated models of biomolecular interaction networks. Genome Res. 13, 2498.

Song, W., Ma, Y.-y., Miao, S., Yang, R.-p., Zhu, Y., Shu, D., Lu, M., Ma, R., Ming, Z.-y., 2018. Pharmacological actions of miltirone in the modulation of platelet function. Acta Pharmacol. Sin.

Szklarczyk, D., Morris, J.H., Cook, H., Kuhn, M., Wyder, S., Simonovic, M., Santos, A., Doncheva, N.T., Roth, A., Bork, P., 2017. The STRING database in 2017: quality-controlled protein–protein association networks, made broadly accessible. Nucleic Acids Res. 45, D362-D368.

Tan, Z., Li, J., Zhang, X., Yang, X., Zhang, Z., Yin, K.J., Huang, H., 2018. P53 Promotes Retinoid Acid-induced Smooth Muscle Cell Differentiation by Targeting Myocardin. Stem Cells Dev 27, 534-544.

Tsoucalas, G., Chevallier, J., Karamanou, M., Papaioannou, T., Sgantzos, M., Androutsos, G., 2016. Historical hallmarks of anticoagulation and antiplatelet agents. Curr. Pharm. Des. 22, -.

Ullah, M.Z., Khan, A.U., Afridi, R., Rasheed, H., Khalid, S., Naveed, M., Ali, H., Kim, Y.S., Khan, S., 2018. Attenuation of inflammatory pain by puerarin in animal model of inflammation through inhibition of pro-inflammatory mediators. Int. Immunopharmacol. 61, 306-316.

Wan, Q., Liu, Z., Yang, Y., 2018. Puerarin inhibits vascular smooth muscle cells proliferation induced by fine particulate matter via suppressing of the p38 MAPK signaling pathway. BMC Complement. Altern. Med. 18, 146.

Wang, H., Gu, J., Hou, X., Chen, J., Yang, N., Liu, Y., Wang, G., Du, M., Qiu, H., Luo,

Y., Jiang, Z., Feng, L., 2017. Anti-inflammatory effect of miltirone on inflammatory bowel disease via TLR4/NF-κB/IQGAP2 signaling pathway. Biomed. Pharmacother. 85, 531-540.

Wang, S.B., Jang, J.Y., Chae, Y.H., Min, J.H., Baek, J.Y., Kim, M., Park, Y., Hwang, G.S., Ryu, J.S., Chang, T.S., 2015. Kaempferol suppresses collagen-induced platelet activation by inhibiting NADPH oxidase and protecting SHP-2 from oxidative inactivation. Free Radic. Biol. Med. 83, 41-53.

Wang, Y., Zhu, H., Tong, J., Li, Z., 2016. Ligustrazine improves blood circulation by suppressing Platelet activation in a rat model of allergic asthma. Environ. Toxicol. Pharmacol. 45, 334-339.

Wishart, D.S., Feunang, Y.D., Guo, A.C., Lo, E.J., Marcu, A., Grant, J.R., Sajed, T., Johnson, D., Li, C., Sayeeda, Z., 2017. DrugBank 5.0: a major update to the DrugBank database for 2018. Nucleic Acids Res. 46.

Wu, J.K., Yang, Q., 2018. Effect of leech on lipid metabolism and liver in hyperlipidemia rats. Zhongguo Zhong Yao Za Zhi 43, 794-799.

Wu, J.K., Yang, Q., Li, Y.Y., Xie, D.J., 2017. Effect of leech on VSMCs in early atherosclerosis rats via p38MAPK signaling pathway. China journal of Chinese materia medica 42, 3191-3197.

Wu, L., Qiao, H., Li, Y., Li, L., 2007. Protective roles of puerarin and Danshensu on acute ischemic myocardial injury in rats. Phytomedicine 14, 652-658.

Xing, W., Yonghong, Z., 1998. The clinical application of self-prepared Zhixiong capsule. Shaanxi Zhongyi 19, 421-422 (in Chinese).

Yan, L.P., Chan, S.W., Chan, A.S., Chen, S.L., Ma, X.J., Xu, H.X., 2006. Puerarin decreases serum total cholesterol and enhances thoracic aorta endothelial nitric oxide synthase expression in diet-induced hypercholesterolemic rats. Life Sci. 79, 324-330.

Yang, H., Qin, C., Li, Y.H., Tao, L., Zhou, J., Yu, C.Y., Xu, F., Chen, Z., Zhu, F., Chen, Y.Z., 2016. Therapeutic target database update 2016: enriched resource for bench to clinical drug target and targeted pathway information. Nucleic Acids Res. 44, D1069-D1074.

23

Yang, H.L., Korivi, M., Chen, C.H., Peng, W.J., Chen, C.S., Li, M.L., Hsu, L.S., Liao, J.W., Hseu, Y.C., 2017. Antrodia camphorata attenuates cigarette smoke‐induced ROS production, DNA damage, apoptosis, and inflammation in vascular smooth muscle cells, and atherosclerosis in ApoE‐deficient mice. Environ. Toxicol. 32.

Yu, C., Ji, R., He, Z., Liang, C., Wu, Z., 2013. GW24-e0998 Traditional Chinese Medicine Banxiao Capsule Inhibits the Development of Atherosclerosis Plaques In a Rabbit Model. Heart 99, E82-E83.

Zawada, A.M., Rogacev, K.S., Hummel, B., Grun, O.S., Friedrich, A., Rotter, B., Winter, P., Geisel, J., Fliser, D., Heine, G.H., 2012. SuperTAG methylation-specific digital karyotyping reveals uremia-induced epigenetic dysregulation of atherosclerosis-related genes. Circ. Cardiovasc. Genet. 5, 611-620.

Zhang, L., Zhang, H., Li, X., Jia, B., Yang, Y., Zhou, P., Li, P., Chen, J., 2016. Miltirone protects human EA.hy926 endothelial cells from oxidized low-density lipoprotein-derived oxidative stress via a heme oxygenase-1 and MAPK/Nrf2 dependent pathway. Phytomedicine 23, 1806-1813.

Zheng, J., Liu, B., Lun, Q., Gu, X., Pan, B., Zhao, Y., Xiao, W., Li, J., Tu, P., 2016. Longxuetongluo capsule inhibits atherosclerosis progression in high-fat diet-induced ApoE(-/-) mice by improving endothelial dysfunction. Atherosclerosis 255, 156-163.

Zhou, J., Song, Z., Han, M., Yu, B., Lv, G., Han, N., Liu, Z., Yin, J., 2018. Evaluation of the antithrombotic activity of Zhi-Xiong Capsules, a Traditional Chinese Medicinal formula, via the pathway of anti-coagulation, anti-platelet activation and anti-fibrinolysis. Biomed. Pharmacother. 97, 1622-1631.

Zhou, Y.J., Wang, H., Li, L., Sui, H.H., Huang, J.J., 2015. Inhibitory effect of kaempferol on inflammatory response of lipopolysaccharide-stimulated human mast cells. Yao xue xue bao = Acta pharmaceutica Sinica 50, 702.
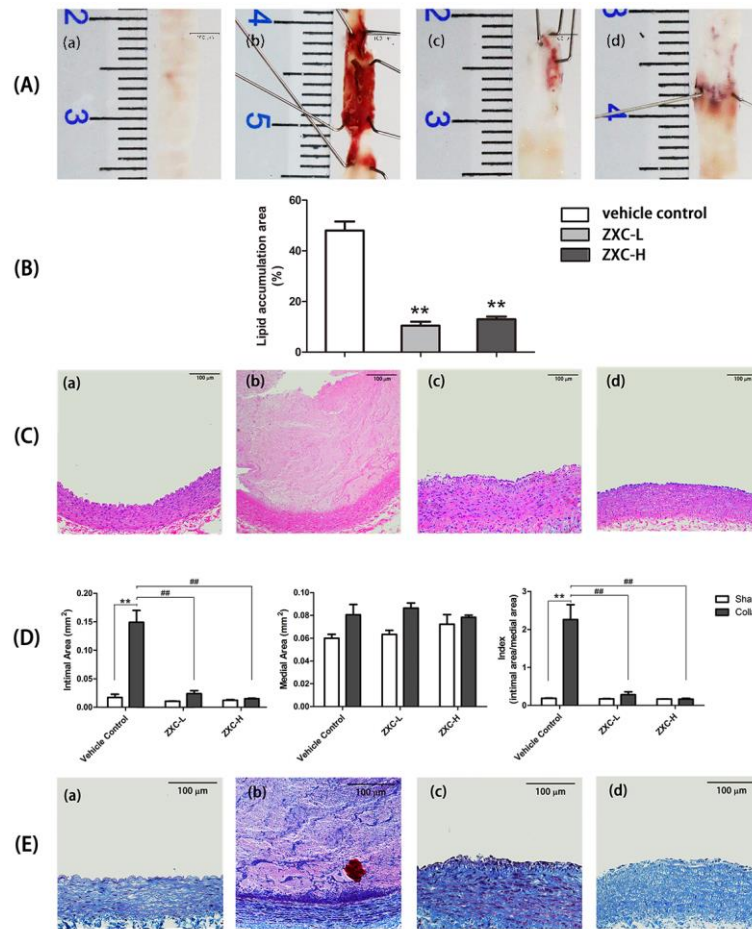
Figure Legends

Fig 1. Histological evaluation of carotid artery atherosclerosis in rabbits.

(A) Representative findings of the carotid artery (operation side) with Sudan IV staining. (B) Quantitative measurement of the lipid accumulation area of Sudan IV staining. **$p < 0.01$ *vs.* vehicle control group. (C) Representative findings of cross-section stained with hematoxylin/eosin. (D) Intimal area and index. **$p < 0.01$ vs. sham-operation side, ##$p < 0.01$ *vs.* vehicle control group (E) Representative findings of cross-section stained with masson-trichrome staining. All results of (B) and (D) are expressed as mean ± SD.(a) blank control group, (b) vehicle control group, (c) ZXC-L group, (d) ZXC-H group
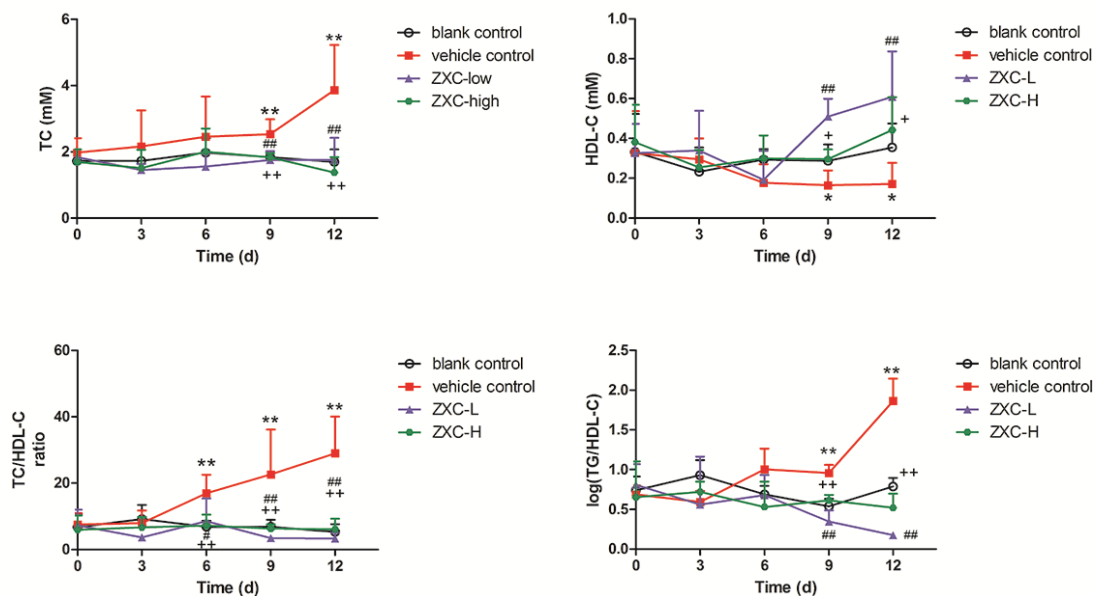
Fig 2. Effects of ZXC on blood lipid level of rabbits during 12 d of high fat diet intake. (A) plasma cholesterol level, (B) plasma HDL-C level, (C) Index of TC/HDL-C, (D) Index of log(TG/HDL-C). All results are expressed as mean ± SD. *$p<0.05$ vehicle control group *vs.* blank control group;**$p<0.01$ vehicle control group *vs.* blank control group; ##$p<0.01$ ZXC-L group *vs.* vehicle control group; +$p<0.05$ ZXC-H group *vs.* vehicle control group; ++$p<0.01$ ZXC-H group *vs.* vehicle control group.
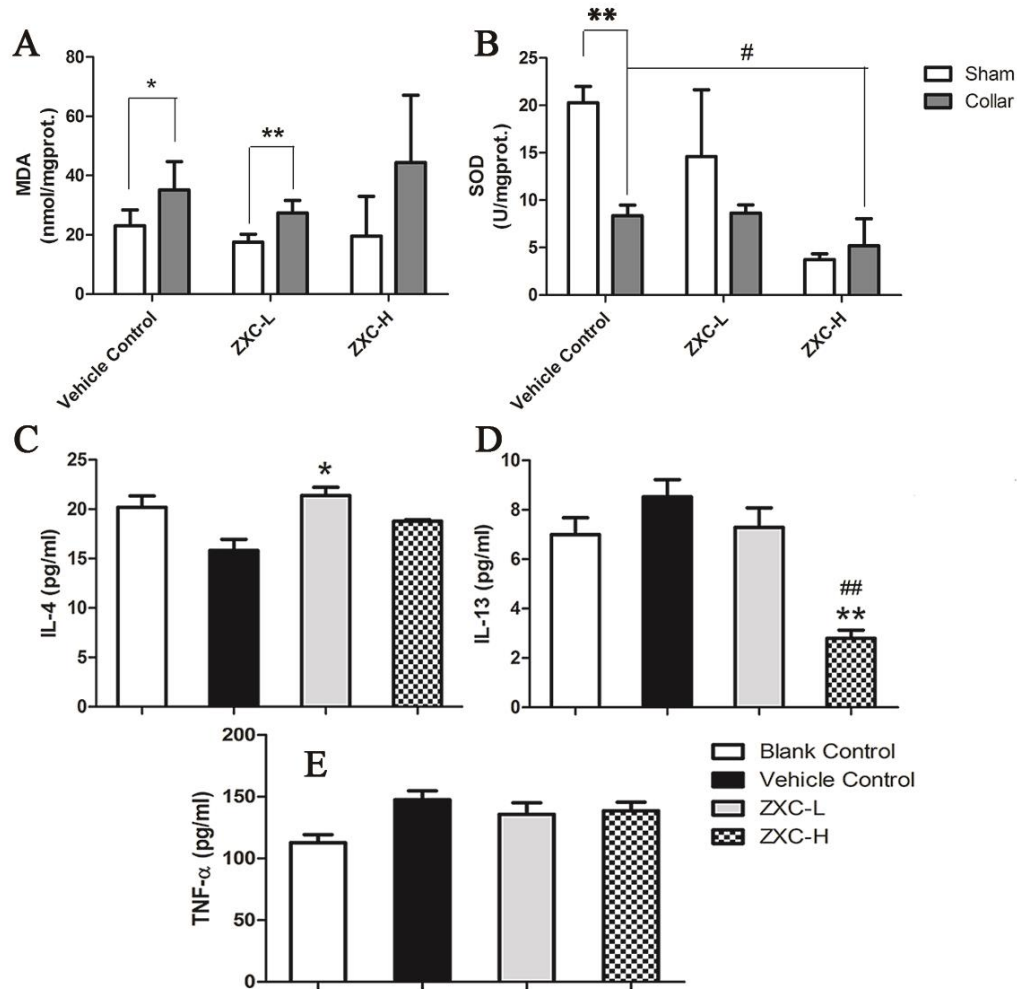
26

Fig 3. Effects of ZXC on (A) MDA level in sham-operated and operated carotid arteries, (B) SOD activity in sham-operated and operated carotid arteries, (C) plasma IL-4 content, (D) plasma IL-13 content, (E) plasma TNF-α content in experiment rabbits. In (A) and (B), *p<0.05 *vs.* sham operation artery, **p<0.01 *vs.* sham operation artery, #p<0.05 *vs.* vehicle control group. In (C), (D) and (E), *p<0.05 *vs.* vehicle control group, **p<0.01 *vs.* vehicle control group, ##p<0.01 *vs.* blank control group.
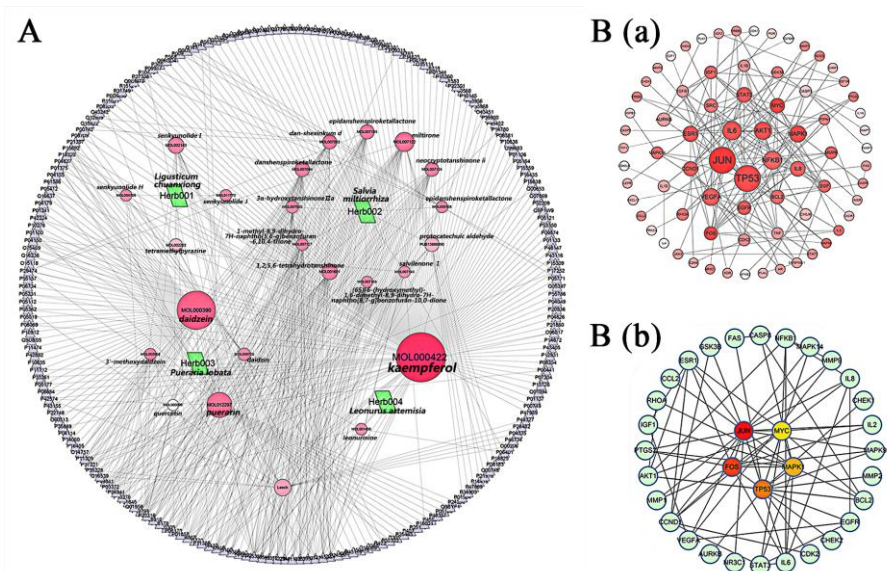
Fig 4. The network construction for ZXC components and targets.

(A) The ZXC herb material (green parallelogram)-component (red circle)-target (purple triangle) network, (B)(a) The protein-protein interaction network constructed by cytoscape, (B)(b) The protein-protein interaction network processed by cytohubba. For the red circles in (A) and (B)(a), the size of a circle is proportional to its betweeness centrality, the saturation of a circle is inversely proportional to its average shortest pathway length. For the circles in (B)(b), the five circles in the center are the five most important targets identified by cytohubba, and the saturation of a circle is inversely proportional to its rank.
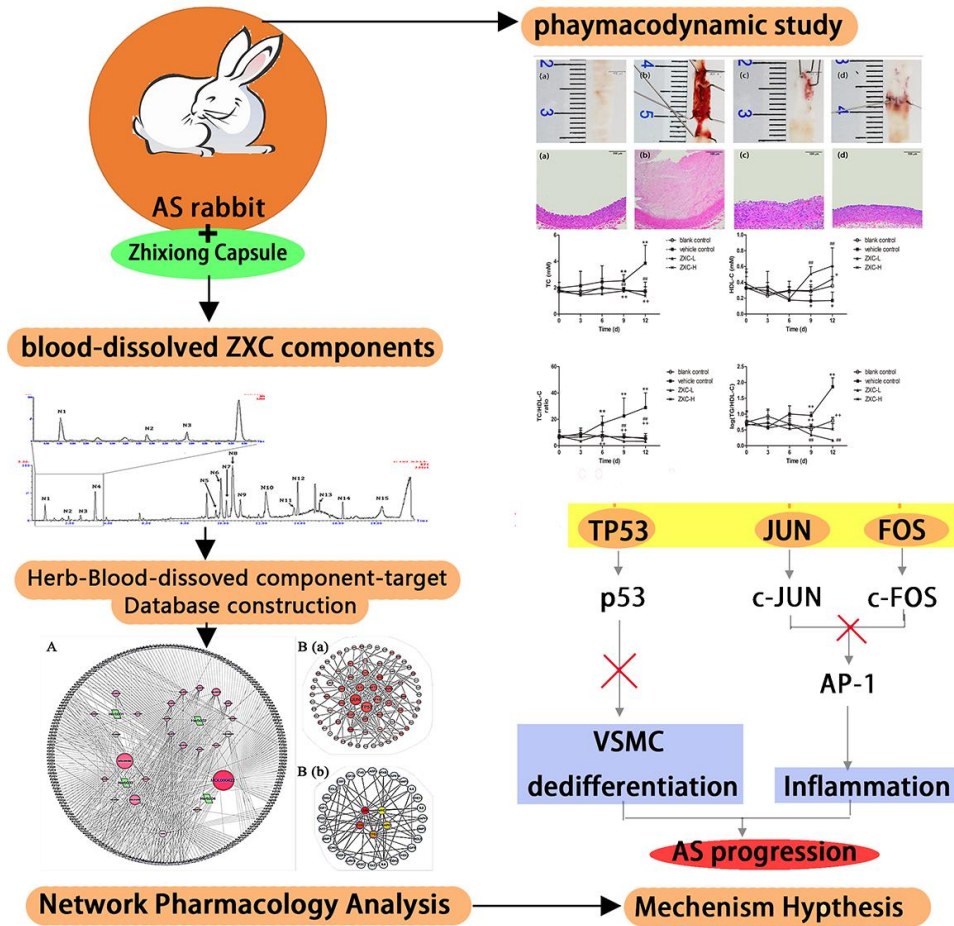
Graphical abstrac

Table 1. The results of network pharmacology analysis

A	Material	Molecular ID	Molecular Name	Average Shortest Pathway Length	Betweeness Centrality
	Leonurus artemisia	MOL000422	kaempferol	1.74895	0.70023
	Pueraria lobata	MOL000390	daidzein	2.47699	0.20965
	Pueraria lobata	MOL012297	puerarin	2.64435	0.10785
	Salvia miltiorrhiza	MOL000712 2	miltirone	2.69456	0.06218
	Leech[a]	——	——	3.09623	0.04278

B	Network Analyzer			Cytohubba	
Target	Average Shortest Pathway Length	Betweenness Centrality		Rank	Target
JUN[b]	*2.04109589*	*0.24642454*		*1*	*JUN[b]*
TP53[b]	*2.26027397*	*0.24410273*		2	FOS
IL6	2.36986301	0.1325048		*3*	*TP53[b]*
NFKB1	2.53424658	0.1259679		4	MAPK1
AKT1	2.32876712	0.11597874		5	MYC

C	ReactomePathway	P-value	HitGenes
	Interleukin-4 and 13 signaling	$1.11*10^{-16}$	PTGS2,CCND1,MYC,AKT1,CCL2,MMP1,MMP2,FOS,MMP9,VEGFA,IL6,BCL2,TP53
	Activation of the AP-1 family of transcription factors	$2.29*10^{-10}$	MAPK9,MAPK1,JUN,FOS,MAPK14
	MAPK targets mediated by MAP kinases	$3.17*10^{-8}$	MAPK9,MAPK1,JUN,FOS,MAPK14
	Transcriptional regulation by TP53	$6.43*10^{-8}$	AURKB,CHEK2,CHEK1,AKT1,JUN,FOS,MAPK14,CDK2,FAS,TP53
	Regulation of TP53 activity	$3.89*10^{-7}$	AURKB,CHEK2,CHEK1,AKT1,MAPK14,CDK2,TP53

A, 5 key components of ZXC; B, 5 key targets of ZXC identified with Network Analyzer and Cytohubba; C, Reactome pathway enrichment results.

[a] Leech was considered as an integrity during this investigation.

[b] JUN and TP53 were identified as the key (hub) targets by comparing betweeness centrality value and by cytohubba plug-in analysis.